THE AMERICAN SOCIETY OF MECHANICAL ENGINEERS
345 E. 47th St., New York, N.Y. 10017

97-GT-83

THE INFLUENCE OF DOWNSTREAM PASSAGE ON THE FLOW WITHIN AN ANNULAR S-SHAPED DUCT

Toyotaka Sonoda, Toshiyuki Arima, Mineyasu Oana
HONDA R&D Co., Ltd.
Saitama, JAPAN

ABSTRACT

Experimental and numerical investigations were carried out to gain a better understanding of the flow characteristics within an annular S-shaped duct, including the influence of the shape of the downstream passage located at the exit of the duct on the flow. A duct with six struts and the same geometry as that used to connect the compressor spools on our new experimental small two-spool turbofan engine was investigated. Two types of downstream passage were used. One type had a straight annular passage and the other a curved annular passage with a similar meridional flow path geometry to that of the centrifugal compressor.

Results showed that the total pressure loss near the hub is large due to instability of the flow, as compared with that near the casing. Also, a vortex related to the horseshoe vortex was observed near the casing. In the case of the curved annular passage, the total pressure loss near the hub was greatly increased compared with the case of the straight annular passage, and the spatial position of the above vortex depends on the passage core pressure gradient. Furthermore, results of calculation using an in-house-developed three-dimensional Navier-Stokes code with a low Reynolds number k-ε turbulence model were in good qualitative agreement with experimental results. According to the simulation results, a region of very high pressure loss is observed near the hub at the duct exit with the increase of inlet boundary layer thickness. Such regions of high pressure loss may act on the downstream compressor as a large inlet distortion, and strongly affect downstream compressor performance.

NOMENCLATURE

A	=	Local cross-sectional area, mm^2
Cp	=	Static pressure recovery coefficient
L	=	Representative axial length of S-shaped duct, 98.6mm (see Fig. 2)
Pt	=	Total pressure, kPa
Ps	=	Static pressure, kPa
R	=	Radius, mm
Tt	=	Total temperature, K
X	=	Axial distance, mm
λ	=	Total pressure loss coefficient

Superscripts and Subscripts

-	=	Time average
hub	=	Inner casing wall
casing	=	Outer casing wall
w	=	Wall
0,1,2	=	Streamwise position (see Figs. 1 & 2)

INTRODUCTION

A swan-neck duct is used to connect the low- and high- pressure compressors of aircraft gas turbine engines. In a small gas turbine, a centrifugal high-pressure compressor is often used. In this case, the swan-neck duct is 'S' shaped due to the aerodynamic design restriction of the centrifugal compressor. Within this duct, flow separation must be avoided to minimize the total pressure loss within the duct. In addition, a uniform flow field at the duct exit must also be achieved. However, it is very difficult to satisfy these various

Presented at the International Gas Turbine & Aeroengine Congress & Exhibition
Orlando, Florida — June 2–5, 1997
This paper has been accepted for publication in the Transactions of the ASME
Discussion of it will be accepted at ASME Headquarters until September 20, 1997

requirements in practice, because the S-shaped duct has struts supporting loads and passages for engine accessories and support systems resulting in a highly complex flow field due to interaction of the duct passage with the struts. Furthermore, the requirements must be fulfilled for a short axial length.

Recently, some studies have been reported on S-shaped ducts (Britchford et al., 1994; Bailey et al., 1995; Bailey and Carrotte, 1996). Their long-term objective is to apply CFD methods to enable the optimum design of S-shaped ducts. Therefore, comprehensive measurements were done using an LDV system under ideal and typical actual engine inlet conditions. However, the S-shaped duct inlet velocity was relatively low and the duct itself was of constant-flow area. Only one radial strut was used in order to assess the effect on performance of placing radial struts within the duct. In this stage of progress in research, it would be worthwhile to investigate the flow within a duct with a more practical configuration and under realistic test conditions. According to the performance test of our centrifugal compressor with an S-shaped duct, the decrease in efficiency was much greater than expected. The S-shaped duct pressure loss seemed to be much larger than that in isolated S-duct performance. Therefore, we have begun research on the flow within an S-shaped duct.

The objectives of this investigation are 1) to study the flow resulting from the interaction of the S-shaped passage with the struts, 2) to investigate the effect on the flow of a downstream passage located at the exit of an S-shaped duct, and 3) to evaluate the reliability of an in-house-developed three-dimensional Navier-Stokes code.

EXPERIMENTAL METHODS

Experimental Facility

A schematic of the S-shaped duct test rig is shown in Fig. 1. Air is supplied by laboratory compressors into a plenum chamber prior to passing through the S-shaped duct, and is exhausted to atmospheric pressure via an exhaust diffuser system set up in the test cell. The detailed configuration of the S-shaped duct is shown in Fig. 2 and Table 1. This duct has the similar geometry as that used to connect the compressor spools on our new experimental small two-spool turbofan engine. The inlet passage upstream of the S-shaped duct has the same geometry as that of the LPC OGV. In Fig. 2, station 1 corresponds to the trailing edge position of the LPC OGV. The inlet Mach number used in this rig is 0.386 ± 0.03, based on the inlet total pressure (station 0) and the mean value of the hub and casing static pressures at station 1.

In order to investigate the effect of the downstream passage on the flow within the S-shaped duct, two different downstream passages were fitted alternatively at the S-shaped duct exit. One has a straight annular passage and the other a curved annular passage with a similar meridional flow path geometry to that of the centrifugal compressor. Static pressure taps are located at various streamwise positions on the hub and the casing, which allow for the estimation of the flow characteristic and the effect of the downstream passage. The circumferential position of these taps corresponds to the midpoint between the struts. Also, on the strut surface, static pressure taps are located at 11%, 44%, and 89% of the strut span. The area ratio (A1/A2) of the S-shaped duct is about 1.2. The S-shaped duct has six struts with NACA 0021 profile geometry, and are canted by 15 degrees to match the S-shaped duct passage. The flows on the strut and the hub/casing surfaces have been visualized using a mixture of titanium dioxide and oleic acid.

Instrumentation

Inlet total pressure and temperature are measured at the center of the plenum chamber (Fig. 1). At the outlet, using the 3-axis traverse mechanism, traverse measurements of pressure were made using a miniature five-hole pressure probe with an overall diameter of 1.5 mm, which was calibrated in advance. The axial position of these measurements (X/L=1.03) nearly corresponding to the centrifugal impeller leading edge (station 2). The outer ring of both straight and curved annular passages moves in the circumferential direction by the 3-axis traverse mechanism. The data are mainly obtained at 8 radial positions traversed along 20 circumferential points. The area traversed corresponds to half of the strut pitch.

Data Reduction

Static pressures along the hub, the casing and the strut surface are given in terms of the pressure recovery coefficient (Cp), while the total pressure loss coefficient between the S-shaped duct inlet (station 1; X/L=0.0) and the duct exit (X/L=1.03; near station 2) is defined as λ.

$$C_p = \frac{P_{s,w} - \overline{P_{s,1}}}{P_{t,1} - \overline{P_{s,1}}}; \qquad \lambda = \frac{P_{t,1} - P_{t,2}}{P_{t,1} - \overline{P_{s,1}}}$$

$$\overline{P_{s,1}} = \frac{1}{2}\left(P_{s,1,\text{casing}} + P_{s,1,\text{hub}}\right)$$

Here, the total pressure at station 1 is the same as the pressure at station 0 in the plenum chamber.

The five-hole pressure probe provides information on total and static pressure as well as flow direction (pitch and yaw angles) and velocity is calculated from these data.

Estimate of Experimental Error

The inlet total pressure probe, static taps and five-hole pressure probe discussed above were connected to a precalibrated differential pressure transducer which had a range of ±98 kPa. The output was read automatically from an integrating digital voltmeter. Total and static pressure measurements were reproducible to within ±10 mm of water. Based on these values, it was estimated that the static pressure recovery and the total pressure loss coefficient were reproducible to within ±0.02 and ±0.01, respectively.

COMPUTATIONAL METHODS

A three-dimensional compressible Navier-Stokes code with a low Reynolds number k-ε turbulent model, Arima et al. (1997), has been applied to the flow within the S-shaped duct. The computational body-fitted grid, for example, used for the S-shaped duct with a curved annular passage, is shown in Fig. 3. Part of the casing grid is omitted to allow a better view of the S-shaped duct with struts. The grid consists of 61 nodes in the strut-to-strut direction, 41 nodes in the spanwise direction, and 156 nodes in the streamwise direction. Calculations have been done under various inlet boundary layer thickness conditions (1.0%, 2.0%, 5% and 10% of the inlet passage height) for the two configurations (the straight annular passage and the curved annular passage). As inlet boundary conditions, standard pressure and temperature were used, and inlet flow direction was along the hub and the casing without swirling. As a Euler solver, Denton's code was also used. Downstream back pressure was adjusted to coincide with the corrected mass flow.

RESULTS & DISCUSSION

Inlet Boundary Layer

The inlet boundary layer thickness was estimated by the assumption of laminar flow (i.e., Blasius flow). The calculated boundary layer thickness is about 0.2 mm at the inlet of the S-shaped duct (Station 1), and it corresponds to about 1% of passage height.

Flow Visualization

Flow has been visualized experimentally and numerically to gain a qualitative understanding of the flow pattern within the S-shaped duct. The representative results for the straight annular duct are shown in Fig. 4. The inlet boundary layer thickness used in calculations corresponds to 1% of passage height. Figure 4(a) shows the flow pattern on the casing. The strut has been removed. The resulting flow pattern on the casing shows a typical horseshoe vortex that forms ahead of the blunt strut leading edge with a stagnation point (saddle point). From this stagnation point, two streamlines emerge and wrap around the strut, while at the trailing edge, two new limiting streamlines form. This pattern is very similar to that observed by Karim Abdulla-Altaii and Raj (1994). They investigated the flow downstream of the corner formed by a blade and a flat plate and called the two limiting streamlines at the trailing edge "wake limiting streamlines". This "wake limiting streamline" in Fig. 4(a) corresponds to the high loss region shown later (Fig. 8) and it shows that there is a very high concentration of vortices adjacent to the casing. While, the wake pattern on the hub is shown in Fig. 4(b). The "wake limiting streamline" observed in the casing is not detected on the hub, experimentally and numerically. This is due to the differences of a streamwise pressure gradient between the casing and the hub field shown later (Fig. 5). There is a slight discrepancy between the experiments and calculations in Fig.4(b). The calculated results show the existence of a week vortex on the hub, while the oil flow results do not.

The horseshoe vortex observed on the casing can also be seen on the hub as shown in Fig. 4(c). As the limiting streamline is traced downstream, it is seen to move toward the strut surface and to be migrating in the spanwise direction on the strut surface. This is due to a streamwise positive pressure gradient on the hub and a spanwise pressure gradient on the strut surface, respectively (see Figs. 5 & 6). The horseshoe vortex on the hub is away from the hub endwall due to the streamwise positive pressure gradient.

There is no separation region on the hub or the casing. However, a small separation region is observed at the trailing edge on the strut surface, (Fig. 4(c)) experimentally and numerically.

On the whole, the calculated results are in good agreement with the experimental results, qualitatively.

Hub and Casing Static Pressure

The hub and casing wall pressure coefficient, Cp, is presented in Fig. 5 for different exit annular passages (i.e., straight or curved annular passage). As the flow follows a curved path within the S-shaped duct, a modification to the static pressure field occurs due to the balance between centrifugal force and radial pressure gradient. Across the first bend, the pressure close to the casing is higher than that adjacent to the hub. However, this situation is reversed at the second bend since the flow returns to the axial direction, as already described by Britchford et al. (1994). The flow experiences a significant positive streamwise pressure gradient in the latter half of the duct on the hub surface as indicated by Cp, which rises from -0.33 to + 0.12. This positive gradient is lower than Britchford et al.'s results (-0.33 to +0.24). Design effort was done to minimize the streamwise positive pressure gradient along the hub in the latter half of the S-shaped duct.

In contrast, the pressure gradient is almost negative adjacent to the casing where Cp decreases from +0.2 to -1.05 along approximately 80% of the duct length. This negative gradient is very large compared to Britchford et al.'s result (+0.2 to -0.26). This is due to the difference in the area ratio and the blockage effect caused by the presence of the six struts.

With the curved downstream annular passage, the static pressure is significantly modified near the exit of the S-shaped duct. The positive pressure gradient is enhanced at the hub, while, the positive pressure gradient is suppressed at the casing.

As shown in Fig. 5, the results calculated using the Euler code (Denton) and the 3-D Navier-Stokes code are in good agreement with experimental results. In particular, the results obtained using our code show excellent agreement. However, it is worthwhile to note that the Denton code is very attractive to aerodynamic designers because of the good agreement within very short times (about 3 minutes of CPU time). In contrast, our code requires about 4 hours on the HONDA Fujitsu VX2.

Strut Static Pressure

The strut wall static pressure coefficient, Cp, is presented in Fig. 6 at 11%, 44% and 89% of the strut span. There are no effect of the downstream passage curvature on the strut surface static pressure between 11% to 89% of the strut span. Although the strut has a two-dimensional profile, there are significant differences in the pressure distribution across the strut span. These differences are mostly due to the differences in the streamwise pressure gradients between the hub and the casing within the S-shaped duct presented earlier, as already described by Bailey et al. (1995). Again, the results calculated using the 3-D Navier-Stokes code are in good quantitative agreement with experimental results, except at one point at about 10% of the axial chord at 11% of the strut span.

Total Pressure Loss Coefficient

Experimental and calculated contours of the total pressure loss coefficient obtained at the S-shaped duct exit (X/L=1.03) are shown in Fig. 7 for (a) the straight annular passage and (b) the curved annular duct. In the calculated contours of the total pressure loss coefficient, each contour value is in order of 5%, 10%, 15%, 20%, 30%, 40%, 50% and 70%. According to the experimental results in the case of the straight annular duct (Fig. 7(a) left), the boundary layer near the hub at the midpoint between the struts is thicker than that near the casing. This is due to the stramwise positive pressure gradient along the hub in the latter half of the duct, as already shown in Fig. 5. It is very interesting that circumferential variation of the total pressure loss is observed adjacent to the casing. The total pressure loss coefficient estimated in the circumferential direction by traverse measurement over a constant-radius surface first increases, then decreases and again increases as the probe moves toward the strut wake. The total pressure loss coefficient shows two maxima in the outer region. This first maxima (about 5 degrees in circumferential position) corresponds to the "wake limiting streamline", as already shown in Fig. 4(a). This deformation of the total pressure loss is due to the horseshoe vortex. The contours of the total pressure loss coefficient for the curved annular downstream passage are shown in Fig. 7(b). The boundary layer thickness near the hub region is greatly increased, as compared with the case of the straight annular downstream passage. This is due to the enhancement of the streamwise positive pressure gradient (see Fig. 5). In contrast, the boundary layer thickness near the casing is slightly decreased due to the suppression of streamwise positive pressure gradient. The remaining regions seem to have only minor

differences.

While, Figure 8 shows the total pressure loss coefficient distribution at various heights near the casing. Although these experimental data are not sufficiently reliable due to the wall effect, qualitative analysis is possible. Two peaks of the pressure loss coefficient (one is due to the strut wake and the other is due to the horseshoe vortex) are clearly revealed in the experiment, and the magnitude of the deformation of the total pressure loss coefficient is larger in the case of the straight annular passage than that in the case of the curved annular passage. This is due to the differences in the passage core streamwise pressure gradient along the casing near the S-shaped duct exit region (see Fig. 5). That is, in the case of the straight passage, the horseshoe vortex moves away from the casing, due to the positive pressure gradient, than that in the case of the curved annular duct (see Fig. 7). A very high concentration of vortices related to the horseshoe vortex is thought to exist adjacent to the casing. This small concentrated vortex may have an adverse effect on the downstream centrifugal compressor performance, such as a large inlet distortion, since, in a real engine, a positive pressure gradient generated on the shroud of an impeller may influence the pressure gradient on the casing of the duct and displace the vortex.

Figure 9 shows the spanwise distribution of mass-averaged total pressure loss coefficient. The total pressure loss near the hub in the case of the curved annular downstream passage is greatly increased due to the enhancement of the streamwise positive pressure gradient, as compared with the case of the straight annular passage. On the other hand, the total pressure loss near the casing in the case of the curved annular downstream passage is reduced due to the suppression of the streamwise positive pressure gradient, as compared with the case of the straight annular passage. Therefore, the difference of the overall mass flow averaged total pressure loss ($\bar{\zeta}$, all) for each configuration is not so large.

The calculated results do not clearly show the concentrated vortex near the casing as a vortex core in the form of total pressure loss coefficient. In comparing the experimental and calculated results, there are discrepancies in the levels of loss in the wake. Both results, however, indicate the same overall behavior.

Secondary Flow Vectors

Experimental and calculated secondary flow vectors obtained for the S-shaped duct exit (X/L=1.03) are shown in Fig. 10 for (a) the straight annular passage and (b) the curved annular duct. Experimental results of velocity vectors near the hub and the casing have been omitted from these figures due to the high radial gradient of the total pressure. In the case of the straight annular passage (Fig. 10(a)), the experimental and calculated results of the secondary vectors indicate radially inward flow. In contrast, in the case of the curved annular passage, the vectors indicate radially outward flow due to the hub passage curvature (Fig. 10(b)). On the whole, the experimental and calculated results show good qualitative agreement. It is very interesting that the vortical motion (clockwise) of the horseshoe vortex is clearly revealed near the casing by the calculations (Fig. 10(a)). However, in the case of the curved annular passage (Fig. 10(b)), it is very difficult to reveal the above vortical motion due to the reduction of the streamwise positive pressure gradient along the casing in the S-shaped duct exit (see Fig. 5) and due to the hub passage curvature (the magnitude of the radially outward flow vectors). In this calculation, the inlet boundary layer is very thin (i.e., 1% of passage height). If the inlet boundary layer is thicker, a vortical motion of the horseshoe vortex near the hub will be more distinct. The features of secondary flow vectors downstream of X/L=1.03 are shown in Fig. 11. The inlet boundary layer thickness is 10% of the passage height. The formation of vortical motion (counter clockwise) related to the horseshoe vortex is more clearly captured at X/L=1.03. Furthermore, the vortices grow with increasing distance from the strut and that, at X/L=1.20, a large vertical vortex appears at mid-passage.

Effect of Inlet Boundary Layer Thickness

As already described, the inlet boundary layer of our S-shaped duct is estimated to be only about 1% of the passage height due to the high acceleration rate. This value is very different from that for real engines. Therefore, it is worthwhile to calculate the effect of the inlet boundary layer thickness on the flow field within the S-shaped duct. Figure 12 shows the variation of the total pressure at X/L=1.03 for (a) the straight annular passage and (b) the curved annular passage. As the inlet boundary layer becomes thicker, the total pressure loss near the hub and the casing at the midpoint between the struts increases, and at the same time, the higher loss region related to the horseshoe vortex are observed on either side of the strut wake near the hub. These regions of high pressure loss on either side of the strut wake near the hub may act on a downstream compressor as a large inlet distortion, and strongly affect the downstream compressor performance.

Flow Development within S-Shaped Duct

A bird's-eye view of the flow development within the duct with inlet boundary layer thickness of 10% of the passage height is shown in Fig. 13. The contours of the total pressure are shown for the case of the curved annular passage. A low total pressure region near the hub has already started on either side of strut surface at the latter half of the S-shaped duct due to the positive pressure gradient. In contrast, the development of the boundary layer along the casing is suppressed by the negative pressure gradient (see Fig. 5).

CONCLUDING REMARKS

Experimental and numerical investigations were carried out to gain a better understanding of the flow characteristics within an annular S-shaped duct, including the influence of the shape of the downstream passage located at the exit of the duct on the flow. The following conclusions were drawn.

- The total pressure loss near the hub is large due to instability of the flow, as compared with that near the casing. Furthermore, a vortex related to the horseshoe vortex is observed in the form of high loss region near the casing, experimentally.

- In the case of the curved annular downstream passage, the total pressure loss near the hub is greatly increased compared with the case of the straight annular passage, and the spatial position of the above vortex near the casing depends on the passage core streamwise pressure gradient.

- Results of calculations using the three-dimensional Navier-Stokes code with a low Reynolds number k-ε turbulent model are in good agreement with experimental results. However, quantitative discrepancies are observed in the wake region; this is a subject for future study.

- According to the simulation results showing the effect of inlet boundary layer thickness, a region of very high pressure loss is generated near the hub. This is due to the formation of the horseshoe vortex related to the inlet boundary layer thickness. Such regions of high pressure loss may act on the downstream compressor as a large inlet distortion, and strongly affect the downstream compressor performance.

The phenomena observed in this investigation may be different when the downstream flow field is controlled by an impeller. Therefore, we are going to investigate the flow of S-shaped duct with a downstream impeller, in near future.

ACKNOWLEDGEMENTS

The authors thank HONDA R&D Co., Ltd. for permission to carry out this study and to publish this work.

REFERENCES

Arima, T., Sonoda, T., Shirotori, M., Tamura, A., and Kikuti, K., 1997, "A Numerical Investigation of Transonic Axial Compressor Rotor Flow Using a Low Reynolds Number k-ε Turbulence Model.". To be presented at ASME TURBO EXPO '97.

Bailey, D. W. and Carrotte, J. F., 1996, "The Influence of Inlet Swirl on the Flow within an Annular S-Shaped Duct", ASME Paper No. 96-GT-60.

Bailey, D. W., Britchford, J. F., Carrotte, J. F., and Stevens, S. J., 1995, "Performance Assessment of an Annular S-Shaped Duct", ASME Paper No. 95-GT-242.

Britchford, K. M., Carrotte, J. F., Stevens, S. J., and McGuirk, J. J., 1994 "The Development of the Mean Flow and Turbulence Structure in an Annular S-Shaped Duct", ASME Paper 94-GT-457.

Denton, J. D., 1985 "The Calculation of Fully 3D Flow Through Any Type of Turbomachine Blade Row", AGARD Lecture Series - 3D Computational Techniques Applied to Internal Flows in Propulsion Systems, AGARD LS 140.

Karim Abdulla-Altaii, A., and Raj, R. S., 1994, "Secondary Flow Development Downstream of a Blade Endwall Corner", ASME Paper No. 94-GT-459.

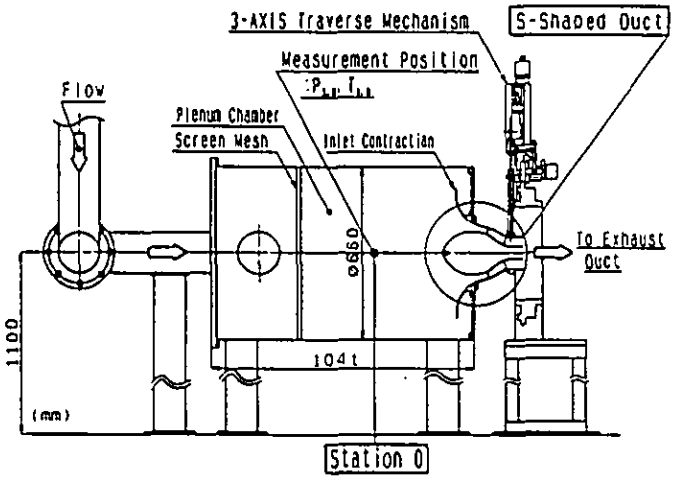

Fig. 1 Schematic Test Rig

Table 1 Flow Path Dimension of S-shaped Duct

X(mm)	R(mm)			
	Hub		Casing	
	Straight	Curved	Straight	Curved
-8.60	81.89	—	103.01	—
0.00 (Stn 1)	79.66	—	100.77	—
3.44	78.51	—	99.98	—
9.40	75.70	—	98.39	—
15.02	72.37	—	96.53	—
22.59	67.05	—	93.60	—
29.19	61.92	—	90.72	—
36.07	56.43	—	87.36	—
42.81	51.22	—	83.71	—
48.97	46.71	—	80.02	—
55.91	42.07	—	75.76	—
62.17	38.33	—	72.19	—
69.36	34.60	—	68.44	—
75.23	31.98	—	65.93	—
83.77	28.88	—	63.33	—
90.06	27.23	—	62.26	—
93.49	26.66	—	61.97	—
95.98	26.51	—	61.87	—
98.59 (Stn 2)	↑	26.87	↑	61.87
100.97	↑	27.53	↑	61.87
108.98	↑	30.04	↑	62.64
116.61	↑	33.01	↑	65.20
125.36	↑	37.39	↑	71.56
131.42	↑	41.35	↑	79.50
137.78	↑	46.82	—	—
143.08	↑	53.31	—	—
149.24	↑	67.23	—	—

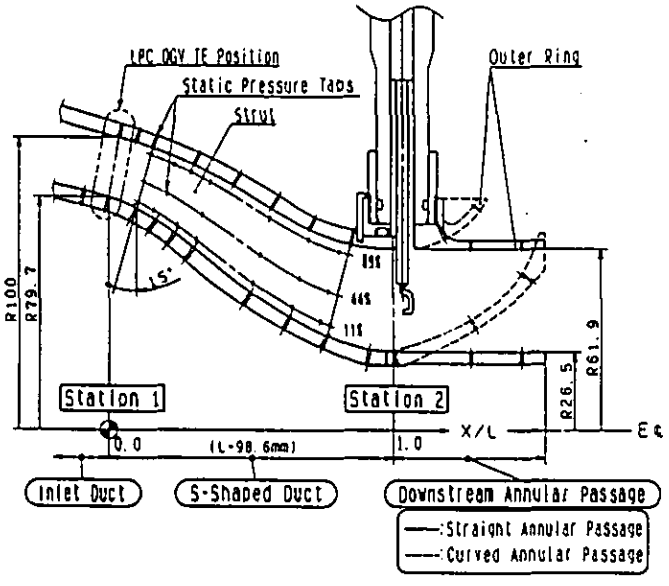

Fig. 2 S-Shaped Duct Geometry and Downstream Annular Passage

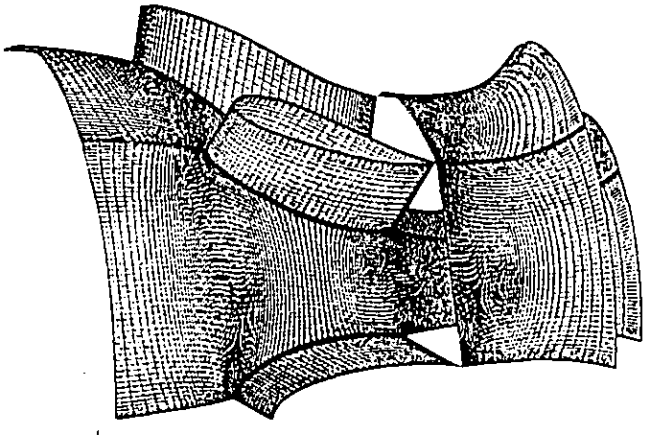

Fig. 3 Computational Grid for S-Shaped Duct

Experiment

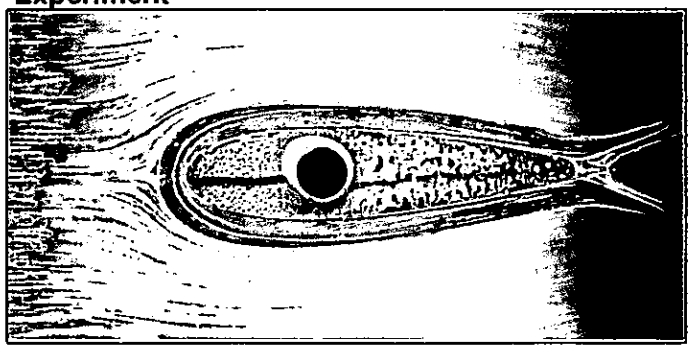

Calculation

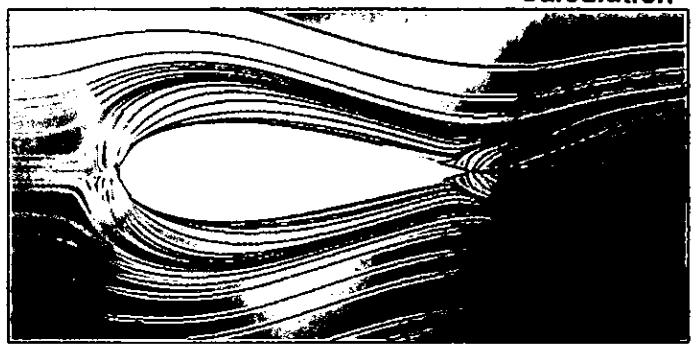

Fig. 4(a) Flow Pattern along Casing

Experiment

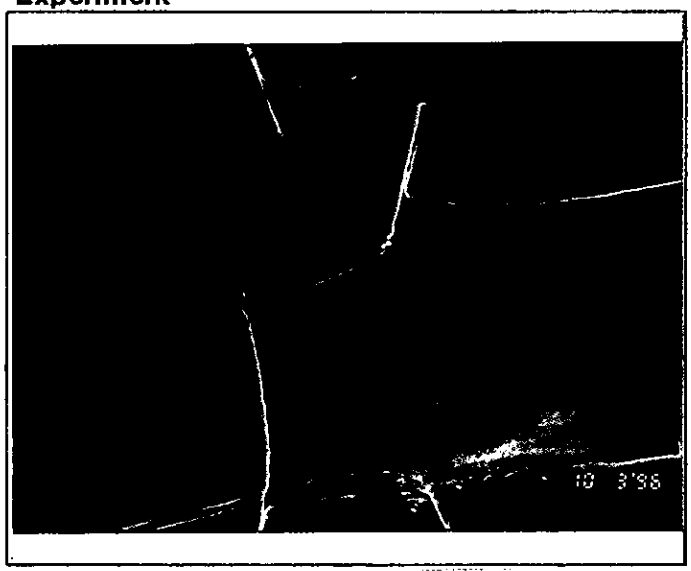

Calculation

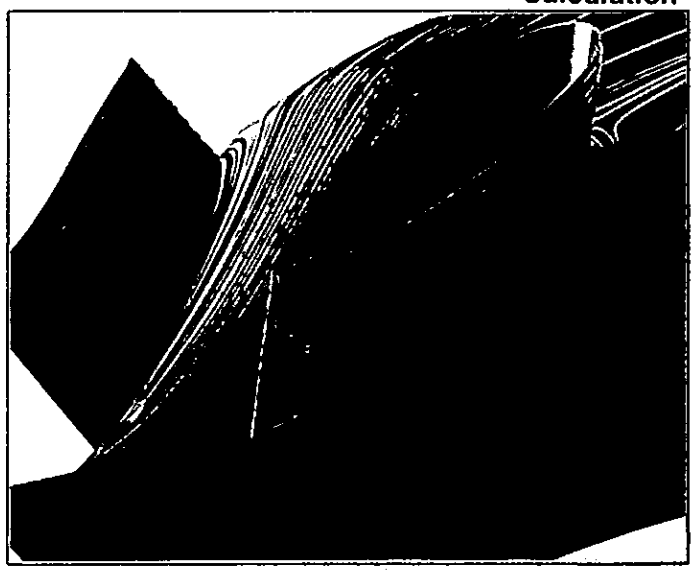

Fig. 4(b) Flow Pattern along Hub

Experiment

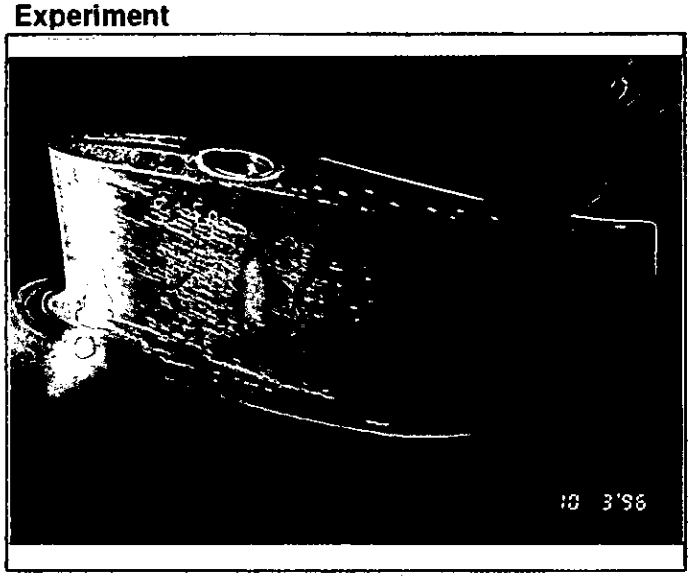

Calculation

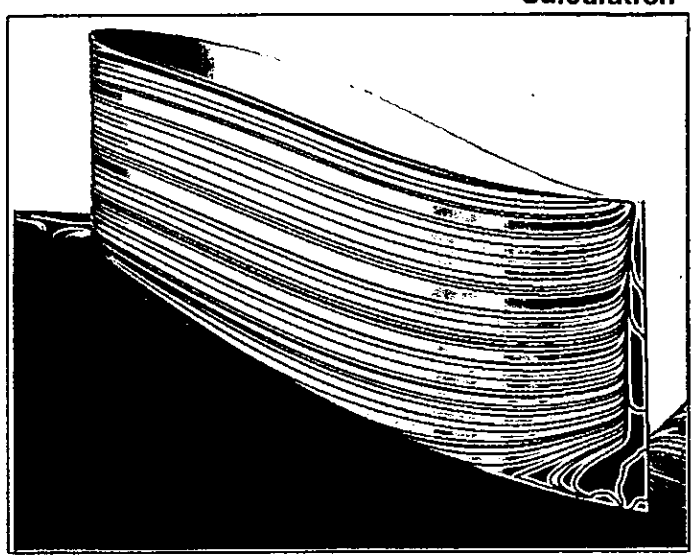

Fig. 4(c) Flow Pattern along Strut Surface

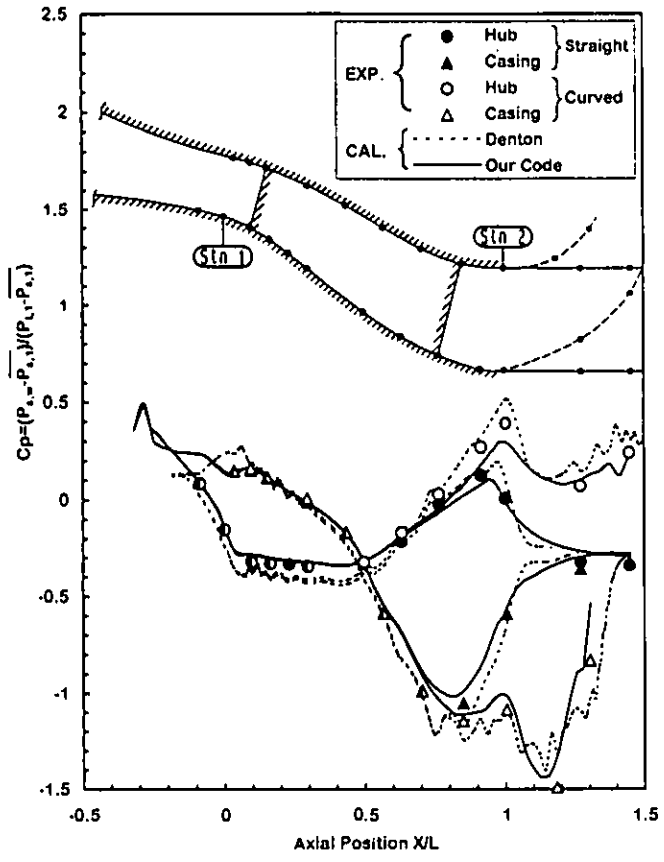

Fig. 5 Static Pressure Distribution on Hub and Casing

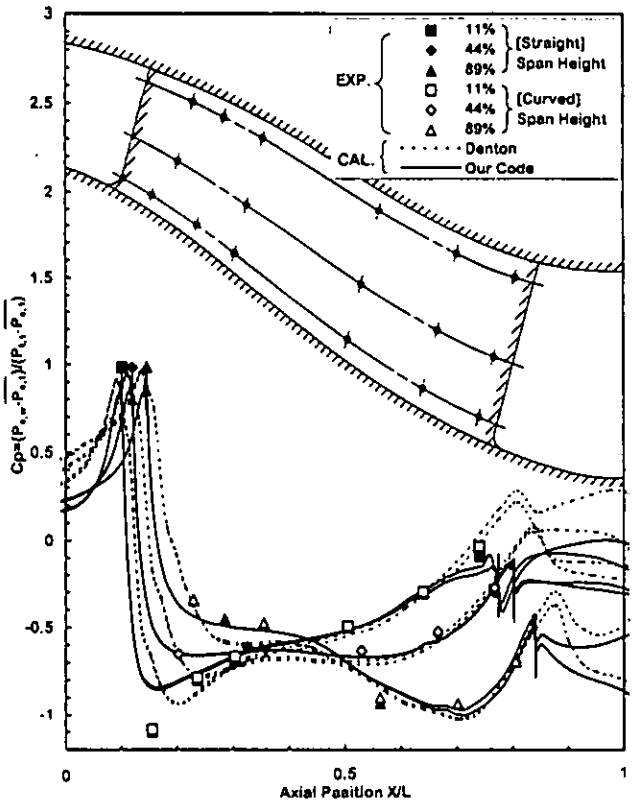

Fig. 6 Static Pressure Distribution on Strut Surface

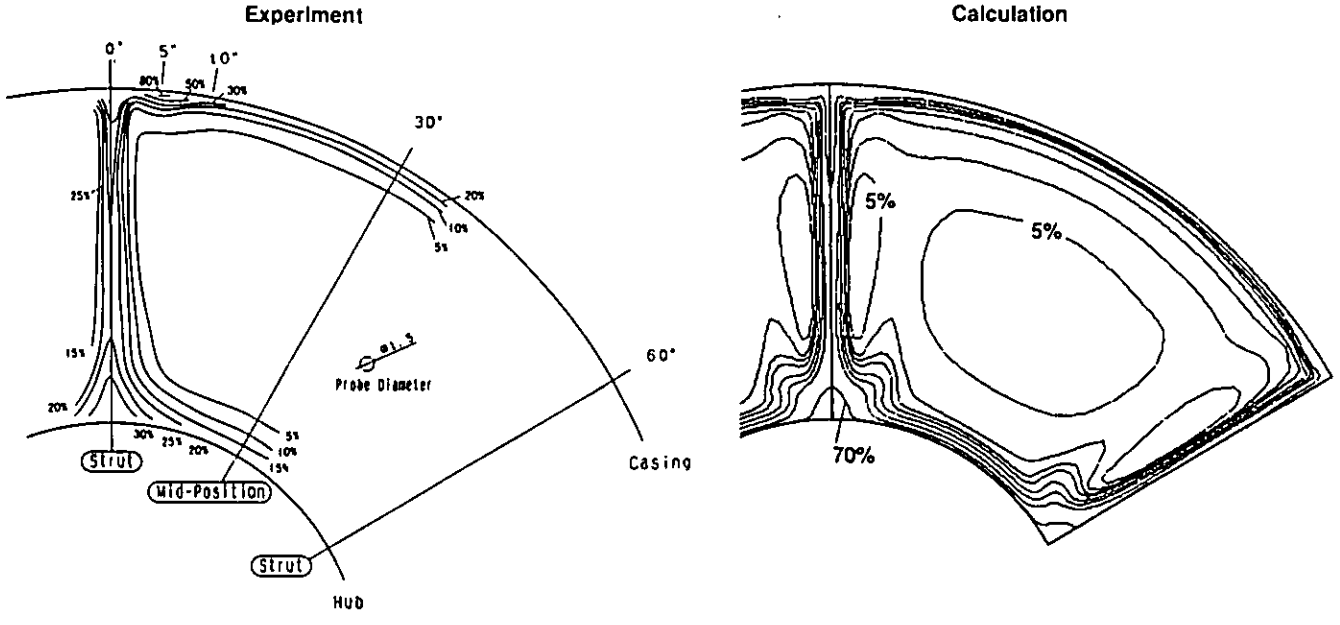

Fig.7 (a) Total Pressure Loss Coefficient Contours for the Case of the Straight Annular Passage

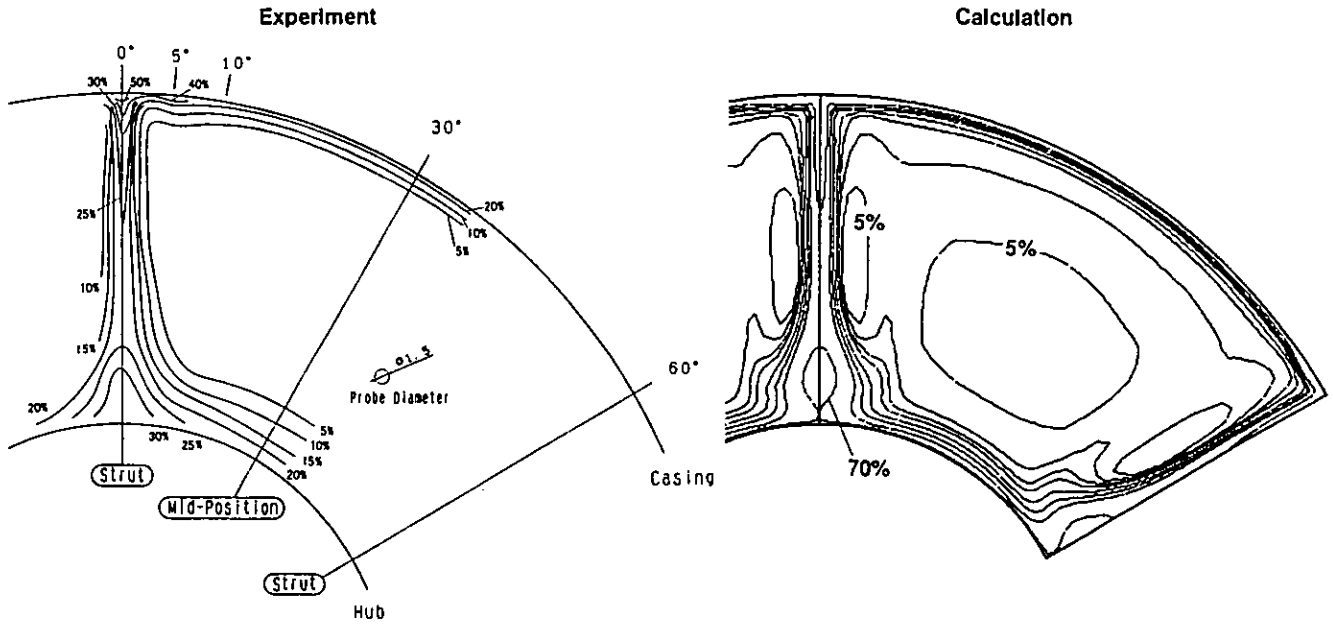

Fig.7 (b) Total Pressure Loss Coefficient Contours for the Case of theCurved Annular Passage

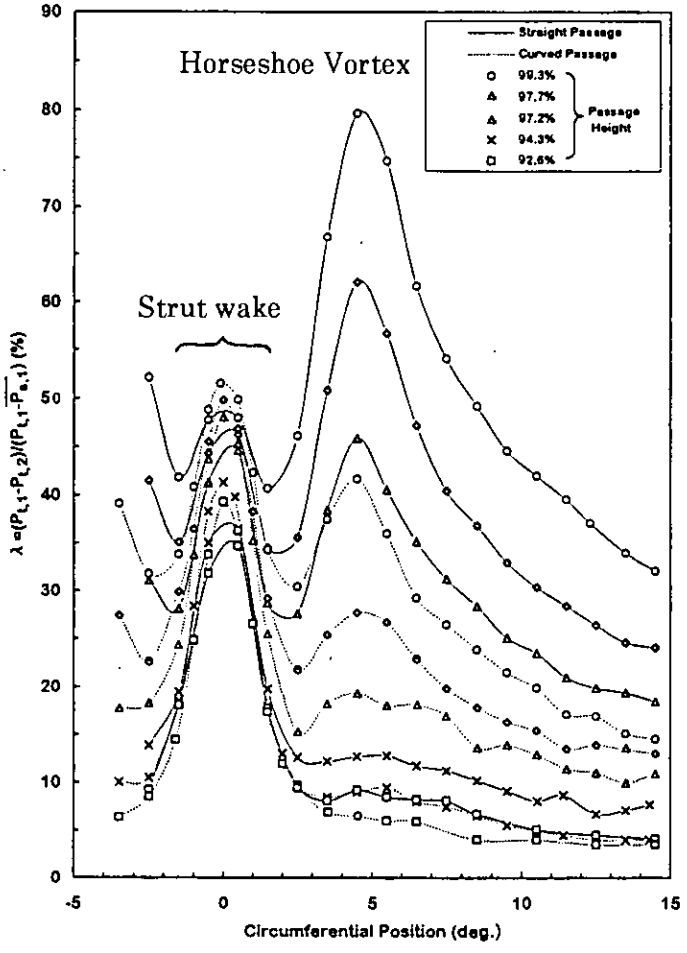

Fig. 8 Total Pressure Loss Distribution at various heights near Casing

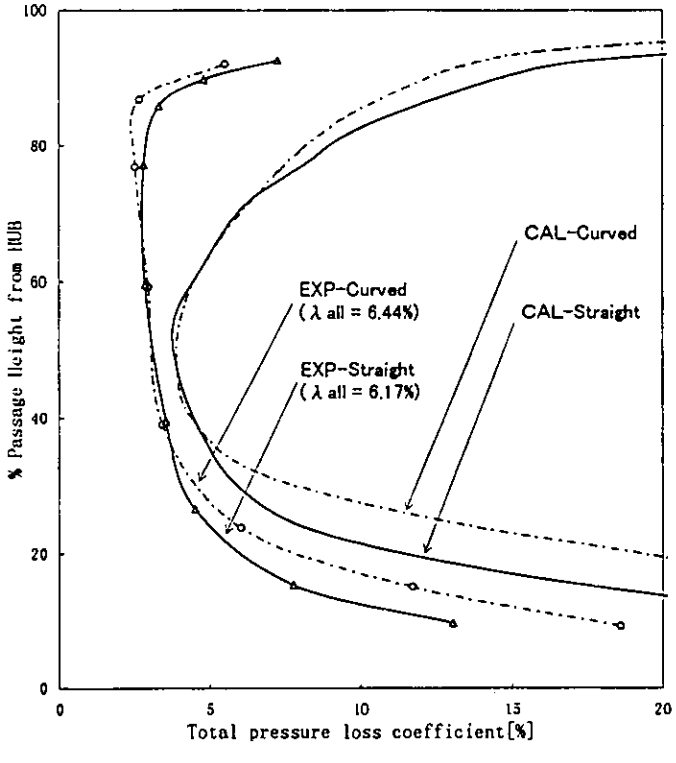

Fig. 9 Spanwise Distribution of Mass-Averaged Total Pressure Loss Coefficient

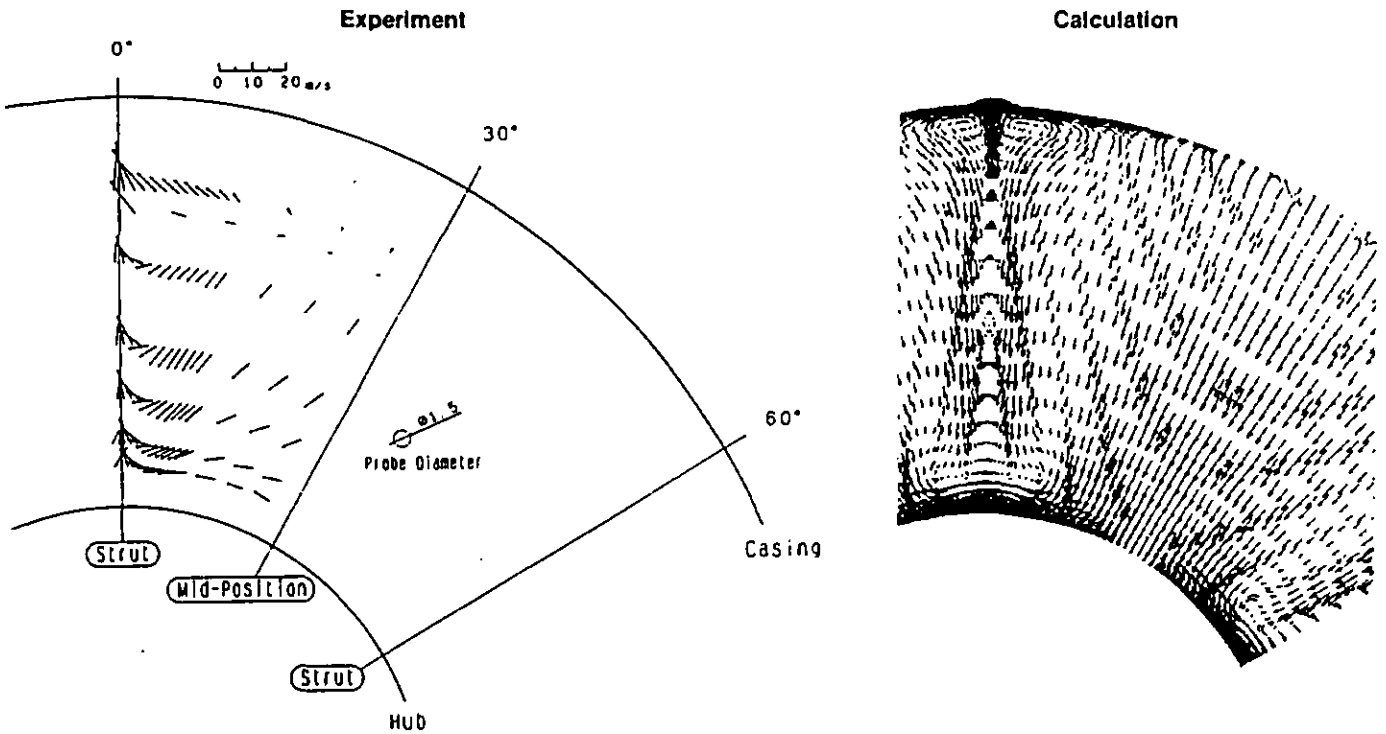

Fig. 10(a) Secondary Flow Vectors for the Case of the Straight Annular Passage

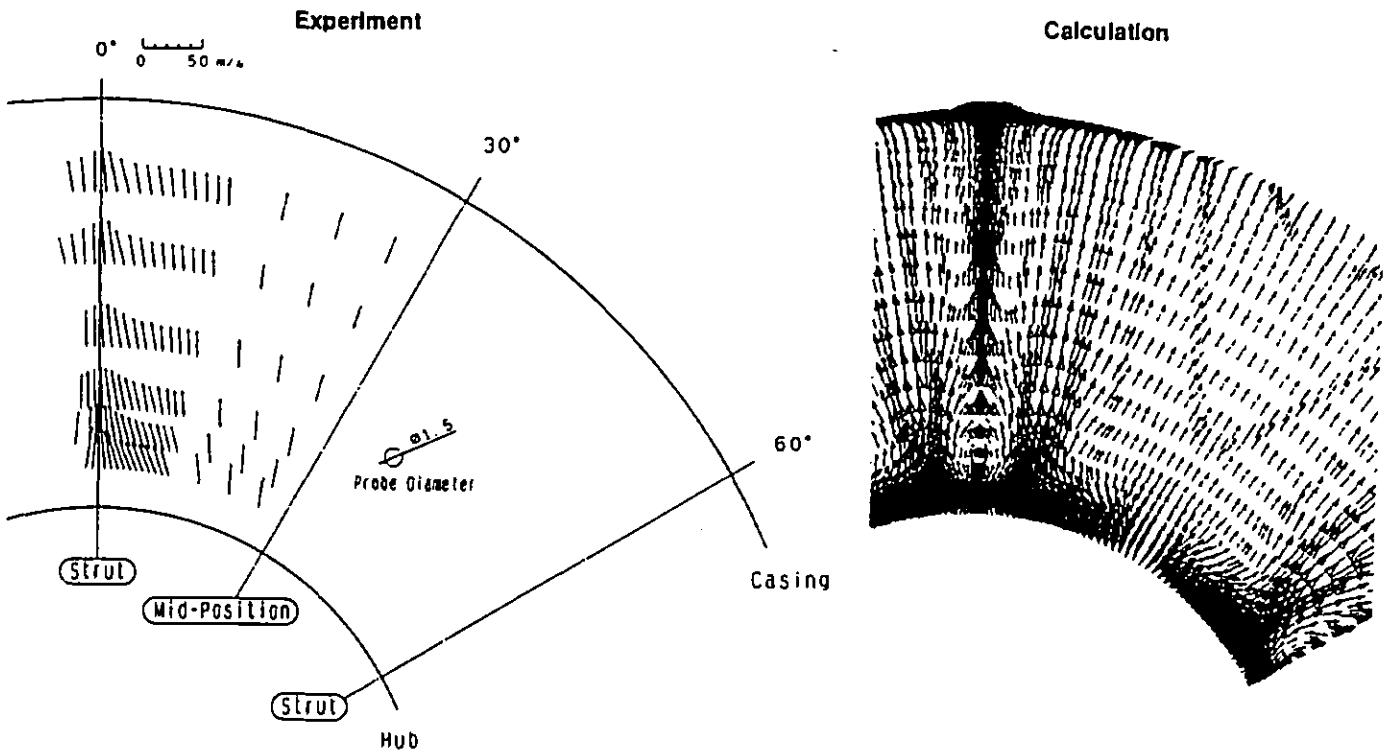

Fig. 10(b) Secondary Flow Vectors for the Case of the Curved Annular Passage

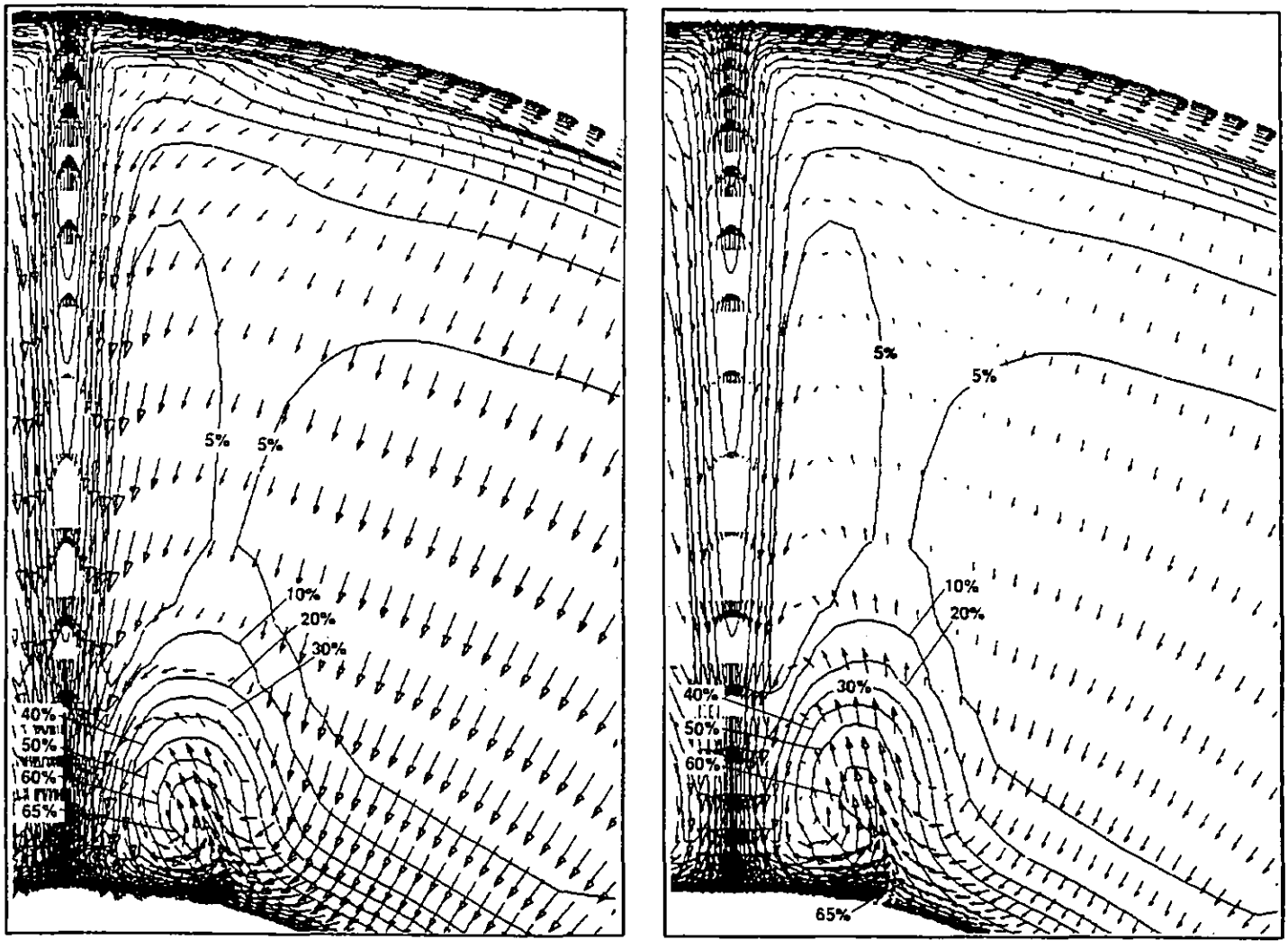

X/L=1.03 X/L=1.20

Fig.11 Formation of Vortical Motion for the Case of Straight Annular Passage (Inlet Boundary Layer Thickness : 10% of Passage Height)

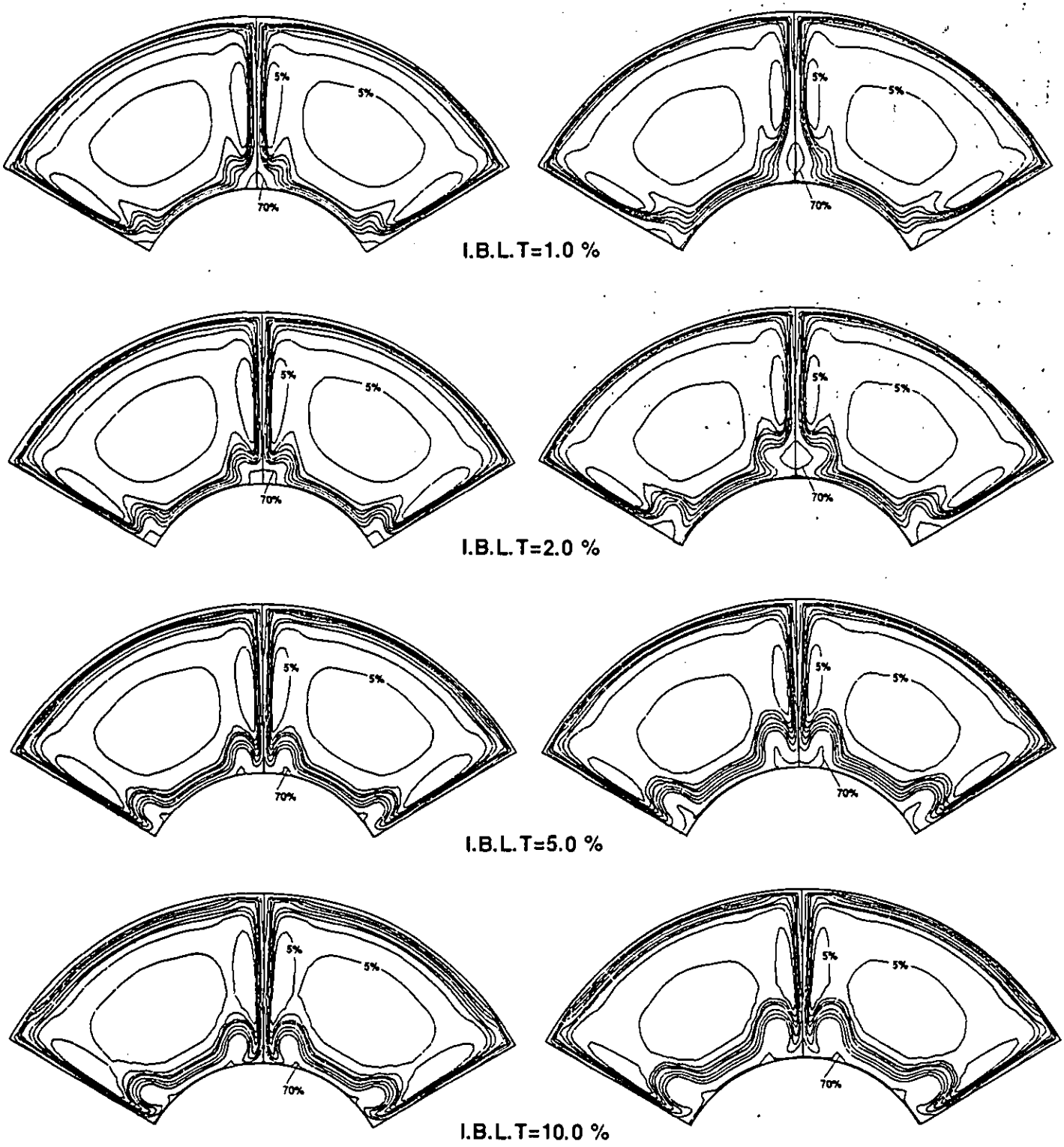

(a) Straight Annular Passage (b) Curved Annular Passage

Fig.12 Effect of Inlet Boundary Layer Thickness on Total Pressure Loss Contours

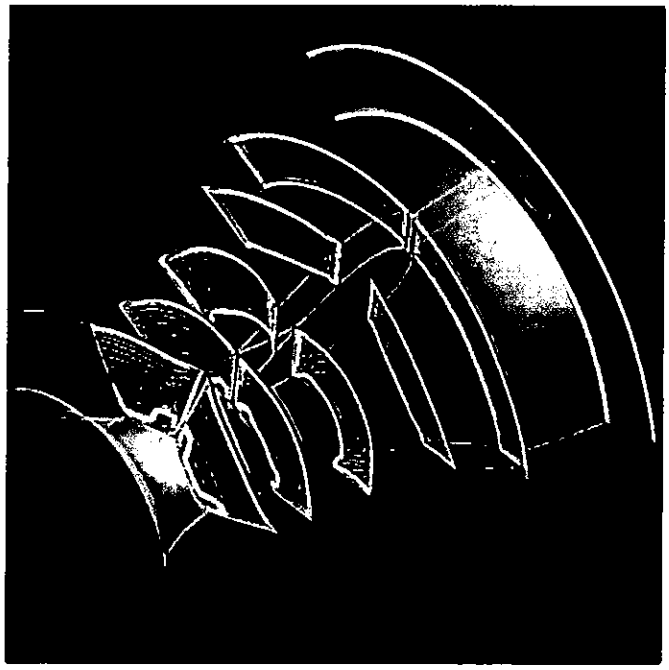

Fig. 13 Bird's-Eye View of Flow Development within an Annular S-Shaped Duct (Inlet Boundary Layer Thickness: 10% of Passage Height)